Journal of Zhejiang University-SCIENCE A (Applied Physics & Engineering) 2023 24(5):432-449
www.jzus.zju.edu.cn; www.springer.com/journal/11582
E-mail: jzus_a@zju.edu.cn

Research Article

https://doi.org/10.1631/jzus.A2200340

General variational solution for seismic and static active earth pressure on rigid walls considering soil tensile strength cut-off

Shiguo XIAO[1,2]✉, Yuan QI[2], Pan XIA[3]

[1]*Key Laboratory of High-Speed Railway Engineering, Ministry of Education, Southwest Jiaotong University, Chengdu 610031, China*
[2]*School of Civil Engineering, Southwest Jiaotong University, Chengdu 610031, China*
[3]*Department of Geological Engineering, Southwest Jiaotong University, Chengdu 610031, China*

Abstract: According to the limit equilibrium state of soils behind rigid walls and the pseudo-static approach, a general closed-form solution to seismic and static active earth pressure on the walls, which considers shear and tension failure of the retained soil, is put forward using a variational calculus method. The application point of the active resultant force specified in the proposed method is explained with a clear physical meaning related to possible movement modes of the walls. In respect of the derived nine dependent equations reflecting the functional characteristics of the earth pressure, the proposed method can be performed easily via an implicit strategy. There are 13 basic factors related to the retained soils, walls, and external loads to be involved in the proposed method. The tension crack segment of the slip surface is obviously influenced by these parameters, apart from vertical seismic coefficient and geometric bounds of the surcharge, but the shear slip segment maintains an approximately planar shape almost uninfluenced by these parameters. Noticeably, the proposed method quantitatively reflects that the resultant of the active earth pressure is always within a limited range under different possible movements of the same wall.

Key words: Active earth pressure; Tensile strength cut-off; Variational calculus method; Pseudo-static method; Strip surcharge

1 Introduction

Active earth pressure is an external load on retaining structures, so its determination is very crucial in practice. Coulomb's theory (Coulomb, 1776) and Rankine's theory (Rankine, 1857) are two classical methods for static earth pressure. Based on the former, Mononobe (1924) and Okabe and Member (1924) provided approaches for seismic earth pressure via a pseudo-static method. However, these classical solutions to static or seismic active earth pressure have some limitations due to their assumptions which, in some cases, are different from practical conditions (Wei et al., 2022). So, many researchers have improved or developed further analytical methods for static active earth pressure under uniform surcharge using a simplified limit equilibrium method (Chang, 1997; Wang, 2000), a slip-line method (Peng and Chen, 2013), a kinematical limit analysis method (Soubra and Macuh, 2002), and a soil-arching-effect method (Paik and Salgado, 2003; Li and Wang, 2014; Rao et al., 2016; Xie and Leshchinsky, 2016; Zhou et al., 2018) and, for seismic active earth pressure, using a pseudo-static method (Choudhury and Singh, 2006; Iskander et al., 2013; Han et al., 2016; Krabbenhoft, 2018). Moreover, similar analytical methods for the active earth pressure under strip surcharge (Kim and Barker, 2002; Greco, 2006; Farzaneh et al., 2014; Hou and Shu, 2019) have been proposed. Tensile behavior is one of the significant properties of cohesive soil (Paul, 1961; Spencer, 1968) influencing its slope stability (Utili, 2013; Michalowski, 2017; Park and Michalowski, 2017; Li et al., 2019), but it is not sufficiently involved in the existing computation methods for active earth pressure. Based on a kinematical limit analysis approach, Li and Yang (2019) and Yang and Zhang (2019) analyzed seismic or static active earth pressure on rigid walls considering the existing tension crack or tensile strength cut-off of soils. Nevertheless, the assumed positions of the cracks are not

✉ Shiguo XIAO, xiaoshiguo@swjtu.cn
Shiguo XIAO, https://orcid.org/0000-0003-4648-5149

Received July 10, 2022; Revision accepted Nov. 28, 2022;
Crosschecked Mar. 20, 2023

always the same as the actual ones, and, in most cases, the segment of the computed critical slip surface near the backfill top surface is not completely identical with the vertical crack shape as actually observed. Indeed, the assumption of the critical slip surface of the retained soil in the upper-bound limit analysis is that its shape is usually log-spiral or planar (Chen, 1975), and can be rigorously derived by the variational calculus method (Kopáscy, 1957; Baker and Garber, 1978; Zhang et al., 2016). Compared with the upper-bound limit analysis, the variational method does not assume that the soil obeys the associated flow rule and thus avoids a possible source of computation error.

According to the variational method, de Josselin de Jong (1980) and Puła et al. (2005) analyzed the limit height of the vertical slope of a frictionless soil and the anchorage force of a wall, respectively. Moreover, Luan and Nogami (1997) proposed an explicit variational approach to determine the two limit earth pressures. Li and Liu (2010) provided a further solution to the active earth pressure of a simple model using a similarly explicit solution tactic based on the variational method. Xiao et al. (2021) put forward an implicit solution strategy to solve the variational problem of the earth pressure under strip surcharge. However, they did not consider tensile strength cut-off of the retained soil in their analysis. Chen et al. (2020) coped with the problem by considering the soil tensile strength, but their assumption on the maximum principle stress at the bottom of the tension crack is questionable since the backfill surface is not usually horizontal and the soil is not actually cracked at any point on the surface, which consequently exhibits a unique solution for the application point of the active thrust regardless of the fact that the application point is linked physically with wall movement modes not yet entirely taken into account in the analysis.

In addition, it should be noted that although there are three basic movement modes of a practical rigid wall including translation and rotations about wall heel and toe under the pushing effect of the retained soil, the accurate movement of the wall is not usually obtained in practical engineering since it is a composite motion composed of the translation and either of the two rotations in a complex way. So, the application point determined only according to one of the simple basic movement modes of the practical wall is doubtful. It would be more rational and safe to determine the variation range of the application point by reference to all possible wall movements.

In view of these factors, seismic and static active earth pressure on the rigid walls are generally analyzed in this study based on the limit equilibrium conditions of the retained soil yielding shear and tension failure criteria and the variational extremization. Considering the possible movement modes of the walls, the application point of the active resultant force involved in the proposed method is explainable with clear physical meaning in a new insight. The thrust force and corresponding shear-tension composite slip surface are fully discussed under the condition of the potential lowermost location of its application point. Besides, the possible variation range of the active earth pressure and its application point corresponding to various wall movements can be determined quantitatively.

As shown in Fig. 1, behind a rigid retaining wall there is homogeneous soil with local strip surcharge on its surface. A composite slip surface *BMO* in the soil in the active limit state due to the wall movement is assumed as a vertical tension crack *BM* with depth *d* obeying the maximum normal stress criterion connected with a continuous curved surface *MO* satisfying the Mohr-Coulomb yield criterion. It begins at a random point *B* on the soil surface and ends at the specified point *O* at the wall heel. In the light of the pseudo-static method of seismic analysis, horizontal and vertical seismic forces characterized briefly by corresponding seismic coefficients are uniformly exerted in the soil and strip surcharge.

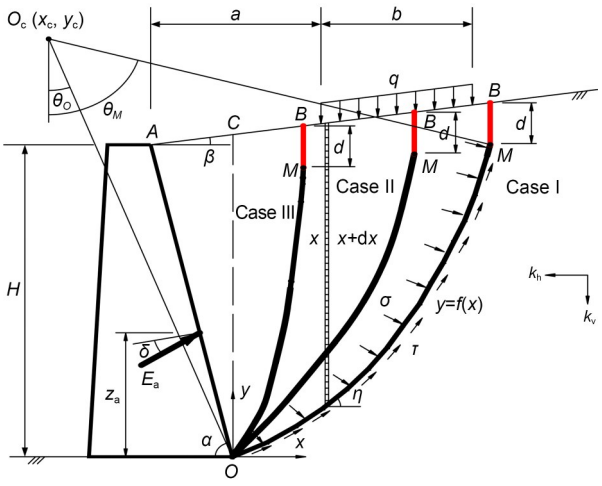

Fig. 1 Analysis model for active earth pressure on a rigid wall. The parameters will be explained in the text

2 Analysis methodology

As shown in Fig. 1, Cases I, II, and III are three possible intersections between the surcharge width and point *B*. The formula of the segment of the sliding surface *MO* is written as $y=f(x)$ with the origin of coordinates set at point *O*, in which *y* and *x* are abscissa and ordinate with reference to the origin *O* in the rectangular coordinate system, where subscripts *M*, *B*, and c represent points *M*, *B*, and O_c, respectively; θ is the dip angle between the radius of the slip surface and the horizontal direction, where subscripts *M* and *O* represent points *M* and *O*, respectively; *f* is the functional relationship between *y* and *x*. Based on the principle of general variational methods finding functions to make the value of quantities depending on their reach extremum (Giaquinta and Hildebrandt, 2004), the problem of resolving the active earth pressure can be described as finding the maximum of the thrust force as a function of the failure surface shape and the normal stress on it under the condition that the soil is in the active limit state.

Based on the Cartesian coordinate system established in Fig. 1 as well as static equilibrium conditions, Eqs. (1)–(3) are the three equilibrium equations for the critical slide body.

$$\overline{H}=\int_{l_{OM}}(\tau\cos\eta-\sigma\sin\eta)\mathrm{d}l-k_{\mathrm{h}}\left[\int_0^{x_M}\gamma(s-y)\mathrm{d}x+F_{\mathrm{q}}+iG_{\mathrm{n}}\right]+E_{\mathrm{a}}\sin(\alpha-\delta)=0, \quad (1)$$

$$\overline{V}=\int_{l_{OM}}(\tau\sin\eta+\sigma\cos\eta)\mathrm{d}l-(1+k_{\mathrm{v}})\left[\int_0^{x_M}\gamma(s-y)\mathrm{d}x+F_{\mathrm{q}}+iG_{\mathrm{n}}\right]+E_{\mathrm{a}}\cos(\alpha-\delta)=0, \quad (2)$$

$$\overline{M}=\int_{l_{OM}}[(\tau\sin\eta+\sigma\cos\eta)x-(\tau\cos\eta-\sigma\sin\eta)y]\mathrm{d}l-(1+k_{\mathrm{v}})\left[\int_0^{x_M}\gamma(s-y)x\mathrm{d}x+M_{\mathrm{qv}}-iM_{\mathrm{nv}}\right]+k_{\mathrm{h}}\left[iM_{\mathrm{nh}}+\int_0^{x_M}\frac{\gamma}{2}(s^2-y^2)\mathrm{d}x+M_{\mathrm{qh}}\right]-E_{\mathrm{a}}\left[z_{\mathrm{a}}\sin(\alpha-\delta)+\frac{z_{\mathrm{a}}}{\tan\alpha}\cos(\alpha-\delta)\right]=0, \quad (3)$$

where $\bar{H}$, $\bar{V}$, and $\bar{M}$ denote the horizontal and vertical resultant forces and resultant moment on a potential slide body, respectively; *l* is the curve length of a shear failure segment of a potential sliding surface *OM*; τ and σ are shear and normal stresses on the shear failure segment, respectively; η is the inclination of a tangent at one point on the potential sliding surface; *k* stands for the seismic acceleration coefficient, where subscripts h and v stand for horizontal and vertical directions, respectively; γ is the unit weight of the soil; *s* is the function of *x* to express the simplified surface of the retained soil; F_{q} denotes the resultant force of the strip surcharge; G_{n} is self-weight of the local soil mass in zone *AOC*; E_{a} represents active earth pressure on the retaining wall; α is the wall back dip angle; δ is the wall-soil friction angle; *M* is the moment with respect to the wall heel point *O*, where subscripts nv, nh, qv, and qh stand for the gravity G_{n}, the horizontal force equal to G_{n} at the centroid of zone *AOC*, the resultant F_{q}, and the horizontal force equal to F_{q} at the midpoint of the strip surcharge; z_{a} is the height of the application point of earth thrust to the wall heel, which can be exhibited as ξH, where the coefficient ξ is the ratio of z_{a} to the wall height *H*. *i* is a calculation index related to the dip angle of wall back and it is equal to 1 if α is not more than 90°. Conversely, it is equal to 0. The other intermediate variables are

$$G_{\mathrm{n}}=\frac{\gamma H^2}{2\tan\alpha}\left(1+\frac{\tan\beta}{\tan\alpha}\right), \quad (4a)$$

$$M_{\mathrm{nv}}=\frac{\gamma H^3}{6\tan^2\alpha}\left(1+\frac{\tan\beta}{\tan\alpha}\right), \quad (4b)$$

$$M_{\mathrm{nh}}=\frac{\gamma H^3}{\tan\alpha}\left(\frac{1}{3}+\frac{\tan\beta}{2\tan\alpha}+\frac{\tan^2\beta}{6\tan^2\alpha}\right), \quad (4c)$$

$$F_q=qb_{\mathrm{e}}, \quad (4d)$$

$$M_{\mathrm{qv}}=qb_{\mathrm{e}}\left(\frac{b_{\mathrm{e}}}{2}+a-\frac{H}{\tan\alpha}\right), \quad (4e)$$

$$M_{\mathrm{qh}}=qb_{\mathrm{e}}\left[H+\left(\frac{b_{\mathrm{e}}}{2}+a\right)\tan\beta\right], \quad (4f)$$

where β is the inclination of the soil surface; *a* is the horizontal offset distance of the strip surcharge *q* to the wall; b_{e} is the effective width of the strip surcharge on the slide body and it is expressed individually corresponding to Cases I, II, and III as:

$$b_{\mathrm{e}}=\begin{cases}b, & x_B\geqslant a-\dfrac{H}{\tan\alpha}+b,\\ x_B+\dfrac{H}{\tan\alpha}-a, & a-\dfrac{H}{\tan\alpha}<x_B<a-\dfrac{H}{\tan\alpha}+b,\\ 0, & x_B\leqslant a-\dfrac{H}{\tan\alpha},\end{cases} \quad (4g)$$

where b is the distribution width of the surcharge on the soil surface.

In fact, x_B=x_M if the tension crack is assumed to be vertical as mentioned above.

From the geometric relationships, we can obtain:

$$\mathrm{d}l=\frac{\mathrm{d}x}{\cos\eta}=\frac{y'\mathrm{d}x}{\sin\eta}, \tag{5}$$

where y' denotes the first-order derivative of $f(x)$.

The classic Mohr-Coulomb criterion assumes that failure occurs if the shear stress on any point in a material reaches a value that depends linearly on the normal stress in the same plane. According to the Mohr-Coulomb yield criterion and substituting Eq. (5) into Eqs. (1)–(3), there are

$$\begin{aligned}\overline{H}=&\int_0^{x_M}[\sigma(\tan\varphi-y')+c-k_{\mathrm{h}}\gamma(s-y)]\,\mathrm{d}x-\\&k_{\mathrm{h}}(F_{\mathrm{q}}+iG_{\mathrm{n}})+E_{\mathrm{a}}\sin(\alpha-\delta)=0,\end{aligned} \tag{6}$$

$$\begin{aligned}\overline{V}=&\int_0^{x_M}[\sigma(y'\tan\varphi+1)+cy'-(1+k_{\mathrm{v}})\gamma(s-y)]\,\mathrm{d}x-\\&(1+k_{\mathrm{v}})(F_{\mathrm{q}}+iG_{\mathrm{n}})+E_{\mathrm{a}}\cos(\alpha-\delta)=0,\end{aligned} \tag{7}$$

$$\begin{aligned}\overline{M}=&\int_0^{x_M}\left\{\sigma[(y'\tan\varphi+1)x-(\tan\varphi-y')y]+\right.\\&\left.c(y'x-y)-(1+k_{\mathrm{v}})\gamma(s-y)x+\frac{k_{\mathrm{h}}}{2}\gamma(s^2-y^2)\right\}\mathrm{d}x-\\&(1+k_{\mathrm{v}})(M_{\mathrm{qv}}-iM_{\mathrm{nv}})+k_{\mathrm{h}}(iM_{\mathrm{nh}}+M_{\mathrm{qh}})-\\&E_{\mathrm{a}}\left[z_{\mathrm{a}}\sin(\alpha-\delta)+\frac{z_{\mathrm{a}}}{\tan\alpha}\cos(\alpha-\delta)\right]=0,\end{aligned} \tag{8}$$

where c and φ are respectively the cohesion and internal friction angle of the retained soil.

Solving for the active earth pressure is substantially searching for the maximum of the force on the wall while the soil is in the active limit state (Coulomb, 1776). Therefore, one can let Eq. (7) be the basic formula and Eqs. (6) and (8) be the two restraint equations including the fundamental variable x, as well as presenting Lagrange multipliers λ_1 and λ_2, to give:

$$\int_0^{x_M}\left(\overline{V}+\lambda_1\overline{H}+\lambda_2\overline{M}\right)\mathrm{d}x=0. \tag{9}$$

In Cases I, II, and III, the intermediate variable m is respectively:

$$\begin{aligned}m=&\sigma\{y'[(\lambda_2x+1)\tan\varphi+(\lambda_2y-\lambda_1)]-\\&(\lambda_2y-\lambda_1)\tan\varphi+(\lambda_2x+1)\}+\\&c[y'(\lambda_2x+1)-(\lambda_2y-\lambda_1)]-\\&(1+k_{\mathrm{v}})\gamma(s-y)(\lambda_2x+1)+\\&k_{\mathrm{h}}\left[\frac{1}{2}\gamma(s^2-y^2)\lambda_2-\gamma(s-y)\lambda_1\right]-\\&\frac{(1+k_{\mathrm{v}})(M_{\mathrm{qv}}\lambda_2-iM_{\mathrm{nv}}\lambda_2+F_{\mathrm{q}}+iG_{\mathrm{n}})}{x_M}+\\&\frac{k_{\mathrm{h}}(M_{\mathrm{qh}}\lambda_2+iM_{\mathrm{nh}}\lambda_2-F_{\mathrm{q}}\lambda_1-iG_{\mathrm{n}}\lambda_1)}{x_M},\end{aligned} \tag{10a}$$

$$\begin{aligned}m=&\sigma\{y'[(\lambda_2x+1)\tan\varphi+(\lambda_2y-\lambda_1)]-\\&(\lambda_2y-\lambda_1)\tan\varphi+(\lambda_2x+1)\}+c[y'(\lambda_2x+1)-\\&(\lambda_2y-\lambda_1)]-(1+k_{\mathrm{v}})[\gamma(s-y)+q](\lambda_2x+1)+\\&k_{\mathrm{h}}\left[\frac{1}{2}\gamma(s^2-y^2)\lambda_2-\gamma(s-y)\lambda_1+\right.\\&\left.qH\left(1+\frac{\tan\beta}{\tan\alpha}\right)\lambda_2+qx\lambda_2\tan\beta-q\lambda_1\right]-\\&\frac{(1+k_{\mathrm{v}})\left[q\left(\frac{H}{\tan\alpha}-a\right)+iG_{\mathrm{n}}\right]}{x_{\mathrm{B}}}+\\&\frac{(1+k_{\mathrm{v}})\left[\frac{q}{2}\left(\frac{H}{\tan\alpha}-a\right)^2\lambda_2-iM_{\mathrm{nv}}\lambda_2\right]}{x_{\mathrm{B}}}+\\&\frac{k_{\mathrm{h}}\left[iM_{\mathrm{nh}}\lambda_2+\frac{q\tan\beta}{2}\left(\frac{H^2}{\tan^2\alpha}-a^2\right)\lambda_2\right]}{x_{\mathrm{M}}}+\\&\frac{k_{\mathrm{h}}\left[qH\left(\frac{H}{\tan\alpha}-a\right)\lambda_2-q\left(\frac{H}{\tan\alpha}-a\right)\lambda_1-iG_{\mathrm{n}}\lambda_1\right]}{x_M},\end{aligned} \tag{10b}$$

$$\begin{aligned}m=&\sigma\{y'[(\lambda_2x+1)\tan\varphi+(\lambda_2y-\lambda_1)]-\\&(\lambda_2y-\lambda_1)\tan\varphi+(\lambda_2x+1)\}+\\&c[y'(\lambda_2x+1)-(\lambda_2y-\lambda_1)]-\\&(1+k_{\mathrm{v}})\gamma(s-y)(\lambda_2x+1)+\\&k_{\mathrm{h}}\left[\frac{1}{2}\gamma(s^2-y^2)\lambda_2-\gamma(s-y)\lambda_1\right]-\\&\frac{(1+k_{\mathrm{v}})(-iM_{\mathrm{nv}}\lambda_2+iG_{\mathrm{n}})-k_{\mathrm{h}}(iM_{\mathrm{nh}}\lambda_2-iG_{\mathrm{n}}\lambda_1)}{x_M}.\end{aligned} \tag{10c}$$

Correspondingly, one can transfer Eq. (9) into

$$E_{\mathrm{a}}=\frac{\int_0^{x_M}m\mathrm{d}x}{(z_{\mathrm{a}}\lambda_2-\lambda_1)\sin(\alpha-\delta)+\left(\frac{z_{\mathrm{a}}}{\tan\alpha}\lambda_2-1\right)\cos(\alpha-\delta)}. \tag{11}$$

Thus, the two Euler equations expressed as Eqs. (12) and (13) should be met to make the function E_a attain its extremum.

$$\frac{\partial m}{\partial \sigma}-\frac{\mathrm{d}}{\mathrm{d}x}\left(\frac{\partial m}{\partial \sigma'}\right)=0, \tag{12}$$

$$\frac{\partial m}{\partial y}-\frac{\mathrm{d}}{\mathrm{d}x}\left(\frac{\partial m}{\partial y'}\right)=0, \tag{13}$$

where σ' is the first-order derivative of σ with respect to x.

Then, as specifically expressed in the electronic supplementary materials (ESM), the functional relationship between the active earth pressure and the critical sliding surface with normal stress on it can be further derived.

For the retained soil with tensile strength cut-off, point M can be regarded as being in both shear failure state satisfying the Mohr-Coulomb yield criterion and tension failure state with horizontally minor principal stress equal to $-R_t$, where R_t is the tensile strength cut-off. As shown in Fig. 2, the normal stress on the slip surface at point M can be derived as:

$$\sigma_M=-R_t(1+\sin\varphi)+c\cos\varphi, \tag{14}$$

where the tensile strength cut-off R_t can be expressed as (Park and Michalowski, 2017):

$$R_t=\psi\frac{2c\cos\varphi}{1+\sin\varphi}, \tag{15}$$

in which ψ is a non-negative coefficient (calibration coefficient) no greater than 0.5 under the condition of non-negative normal stress on the slip surface MO at point M.

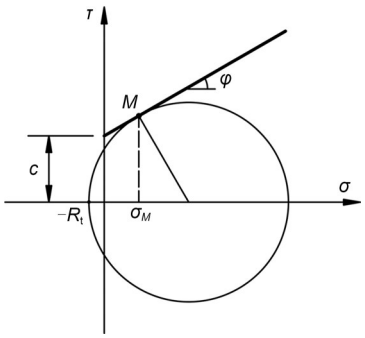

Fig. 2 Illustration of normal stress on the slip surface *MO* at point *M*

Thus, according to Eq. (S10) in the ESM, at point M there is:

$$\frac{K_1\gamma}{1+9\tan^2\varphi}\mathrm{e}^{-\theta_M\tan\varphi}[(1+k_v)(\cos\theta_M+3\tan\varphi\sin\theta_M)-k_h(\sin\theta_M-3\tan\varphi\cos\theta_M)]-\frac{c}{\tan\varphi}+K_2\mathrm{e}^{2\theta_M\tan\varphi}=-R_t(1+\sin\varphi)+c\cos\varphi, \tag{16}$$

where K_1 and K_2 are integral constants.

In total, there are nine independent variables including x_c, y_c, K_1, K_2, θ_O, θ_M, x_M, d, and E_a involved in nine independent equations including Eqs. (S11)–(S17), (S22), and (16). Thus, the nine equations can be solved directly using an implicit approach to accomplish the solutions of the nine variables by a computer program such as MATLAB (The MathWorks, Inc., 2018), in which the inserted function fsolve can be applied to execute the computation and achieve unique solutions easily. The convergence errors of the nine equations can be uniformly adopted as 10^{-5}, which gives satisfactory accuracy and rapid convergence in most cases. So, the active earth pressure and corresponding failure surface under a specified application point can be accurately determined.

It should be noted that a series of possible solutions of E_a can be obtained mathematically under variously specified application point locations. However, the moment on the wall exerted by E_a around its heel or head should be a certain value because it is controlled by the static equilibrium conditions of the wall, and the active earth pressure is the maximum value for those thrust forces in the active limit state of the retained soil, so z_a should be physically adopted within the mathematical solutions to make E_a reach its maximum while keeping that moment on the wall.

In fact, the location of the application point of the active thrust is closely related to the movement modes of the wall which are influenced by some practical circumstances such as foundation conditions and restraints in front of the wall. According to some test results (Niedostatkiewicz et al., 2011), in the case of purely active rotations of the wall around its heel and head as well as translation, volumetric strains of the backfill are relatively concentrated near the heel, head, and middle-lower part of the rigid wall, respectively, which means distribution of compressive stress of the backfill on the

wall is correspondingly focused on those three locations. That is to say, for the purely active rotations of the wall around its heel and head in the tests, the application points of the resultant of the earth pressure are those nearest to and farthest from the wall heel, respectively. However, as shown in Fig. 3, the application point P under pure translation is between the two extreme locations (Fang and Ishibashi, 1986; Hazarika and Matsuzawa, 1996; Matsuzawa and Hazarika, 1996). Therefore, z_a should be physically adopted in its minimum and maximum values within admissible mathematical solutions under pure rotation of the wall around its heel or a point below it and its head or a point above it, respectively. In other words, z_a should be modified within the framework of the theoretically available solutions. If z_a is adopted as between the two extreme values, it means the wall is purely translating or compositely translation-rotation moving to make the backfill be in the active limit state. In brief, different z_a corresponding to the active earth pressures mean different possible movements of the wall, and the earth pressures under different wall movements are naturally different. That is to say, in solving the combined equations in the proposed method, the different z_a specified can cause different results of the active earth pressures, which is reasonable because they physically correspond to different movements of the wall.

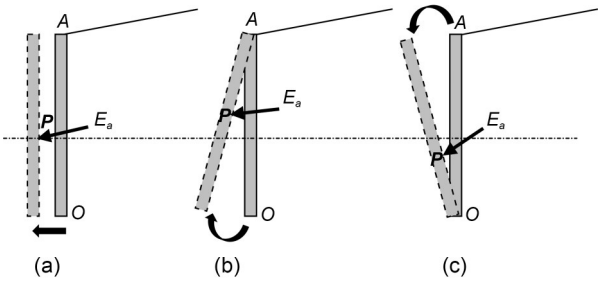

Fig. 3 Relative locations of application point of the active resultant force in three cases: (a) wall translation; (b) wall rotation around the head; (c) wall rotation around the heel

In addition, for the cohesionless backfill or cohesive soil with relatively high surcharge on its top surface, there is no tension crack in the soil behind the wall, which means potential shear failure surfaces in the soil start on its top surface. Namely, point M is totally overlapping with point B. Thus, except for Eq. (16), the nine independent equations are reduced to eight.

3 Applications and verifications

To validate the proposed method, some typical examples including cohesionless and cohesive soil retained by rigid walls are described. For brevity, a coefficient of active earth pressure K_a shown in Eq. (17) is introduced. Also, the application point of the active earth pressure is generally adopted at its lowest value within possible solutions, which corresponds to movement of the wall in rotation about its heel or a point below its heel (substantially a compound movement containing translation and rotation around the heel).

$$K_a = \frac{E_a}{\frac{1}{2}\gamma H^2}. \tag{17}$$

3.1 Some examples of seismic and static earth pressures

Fig. 4 shows comparison of calculation results for some examples of cohesive soil between the proposed method and some existing analytical methods. It indicates that K_a by the proposed method, considering both the Mohr-Coulomb yield criterion and the maximum normal stress criterion (namely, M-C&T), is very close to those from most of the existing methods (Rankine, 1857; Richards and Shi, 1994; Mazindrani and Ganjali, 1997; Shukla et al., 2009; Li and Yang, 2019). However, as can be seen from Fig. 4a, the proposed results are obviously smaller than those by Saran and Prakash (1968) and higher than those by Nian and Han (2013). The reason for the difference between them may be that the self-weight of the slide wedge and cohesion are maximized independently in the former, which causes an overestimated failure state of the retained soil; only local equilibrium conditions near the soil-wall interface are satisfied but the limit equilibrium conditions of the whole slide mass are not considered in the latter, which leads to an underestimated calculation. As expected, K_a by the proposed method, considering only the Mohr-Coulomb yield criterion (namely, M-C), is obviously less than the existing results in most cases. It can be also seen that the critical slide mass by the proposed method (M-C&T) is relatively close to that by upper-bound limit analysis method (Li and Yang, 2019), but the shape and depth of the tension crack are much more adequately reflected by the proposed method (M-C&T) than the

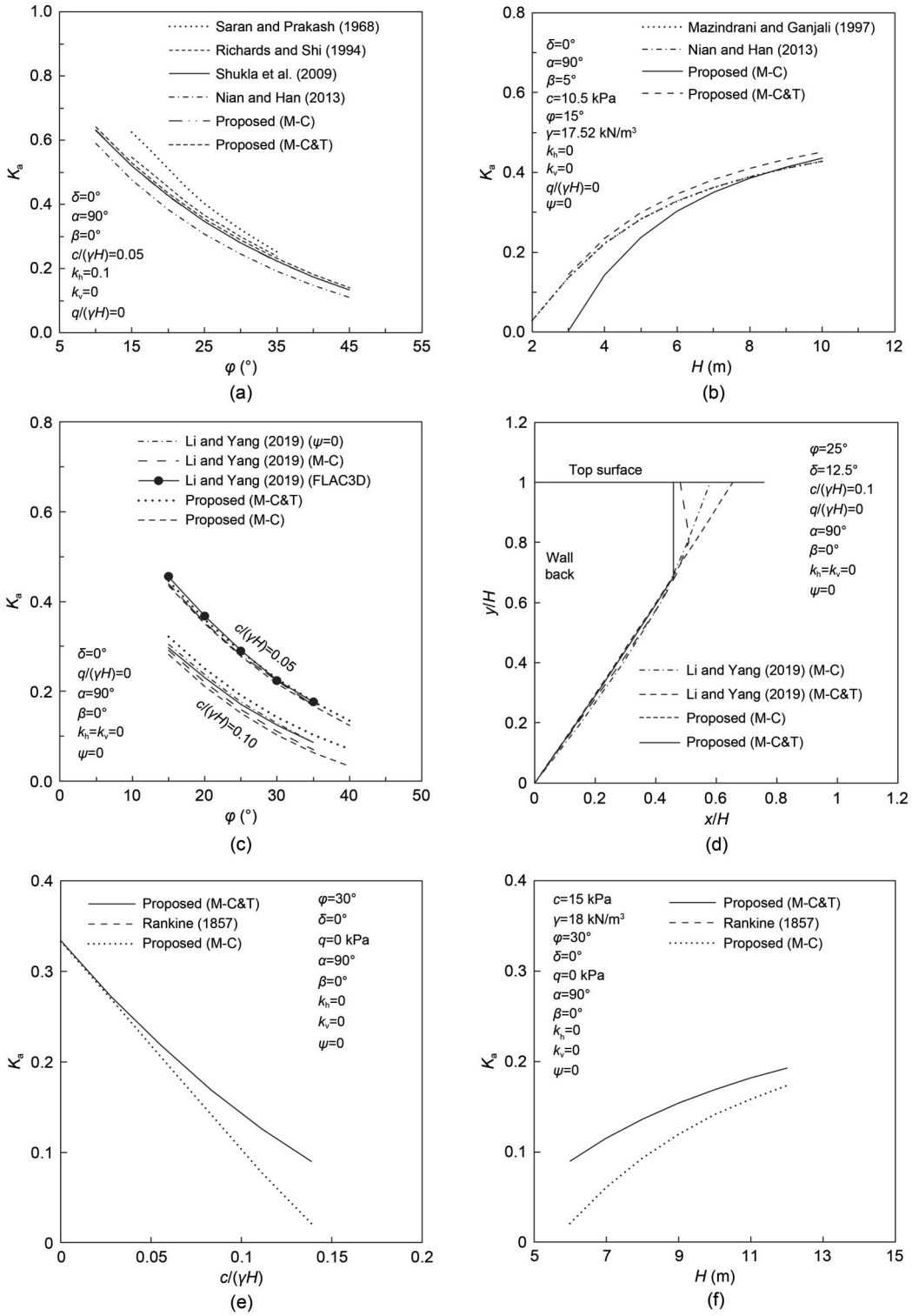

Fig. 4 Comparison of calculation results of cohesive soil between the proposed method and some existing methods for various examples: (a) K_a vs. φ in example 1; (b) K_a vs. H in example 2; (c) K_a vs. φ in example 3; (d) slip surfaces in example 4; (e) K_a vs. $c/(\gamma H)$ in example 5; (f) K_a vs. H in example 6

limit analysis method. Besides, the relationship between K_a and $c/(\gamma H)$ by the proposed method (M-C&T) is obviously nonlinear, which is different from the traditionally linear result (Fig. 4e).

As shown in Fig. 5, seismic active earth pressures of two examples of cohesionless soil are computed using the proposed method (M-C) and some existing methods. One can see in the example with δ=0° the proposed results are identical with those by Shukla et al. (2009) and from the improved Mononobe-Okabe method by Fang and Chen (1995), but they are about 12% higher than those by Nian and Han (2013). For the other example with δ/φ=0.5, the proposed results are also considerably closer to those by Fang and Chen (1995).

3.2 Some examples of static earth pressure with distanced strip surcharge

Active earth pressures under a non-cohesive backfill by different methods are given in Table 1. It can be seen that the proposed results are in good agreement with those of Greco (2006) and Farzaneh et al. (2014). In the case of the relatively high setback distances of the surcharge, the results by the proposed method are visibly higher than those by the Coulomb wedge method (Coulomb, 1776). However, they are averagely 3%–8% smaller than those by the stress distribution approach (Franz G, 1983; Cernica, 1995; MOHURD, 2013) on the basis of the elastic theory. As for the results for a cohesive backfill (Table 2), the proposed earth pressures are relatively close to those by Farzaneh et al. (2014). But the results by the two methods are, on average, 5%–15% smaller than those by the stress distribution approaches. Thus, the existing approaches are more conservative than the proposed method. The reason for that is that the latter is on the basis of a limit state

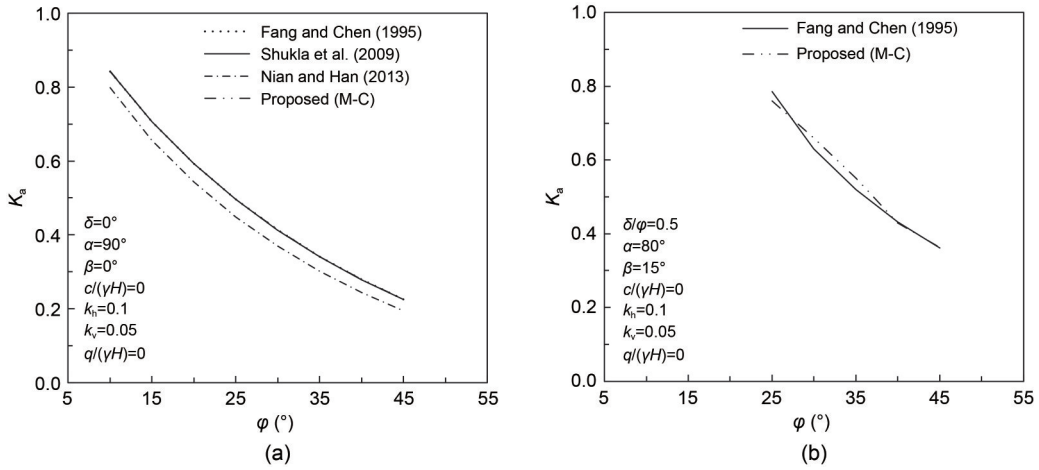

Fig. 5 Comparison of calculation results of cohesionless soil between the proposed method and some existing methods for two examples: (a) K_a vs. φ in one example; (b) K_a vs. φ in the other example

Table 1 Active earth thrusts of non-cohesive soil calculated using different methods (γ=20 kN/m^3, φ=30°, δ=10°, ψ=0, H=10 m, α=90°, and β=0°) (Xiao et al., 2021)

q (kPa)	a (m)	b (m)	Active earth thrust (kN/m)							
			Coulomb (1776)	Franz G (1983)	45° distribution (Cernica, 1995)	45°+φ/2 distribution (MOHURD, 2013)	Greco (2006)	Farzaneh et al. (2014)	Proposed	Ratio ξ
10	2	1	313.4	346.8	336.7	339.1	313.4	314.7	313.5	0.31
20	2	1	318.4	360.3	340.0	344.9	318.4	320.3	318.6	0.32
30	2	1	323.5	373.7	343.3	350.7	323.5	326.1	323.4	0.32
20	4	1	308.5	375.7	340.0	344.9	318.4	320.3	318.7	0.31
50	4	1	308.5	439.2	350.0	362.2	333.8	338.0	333.5	0.30
100	4	1	312.2	545.0	366.7	391.1	362.9	368.9	358.2	0.29
20	3	2	315.2	379.5	346.7	356.4	328.6	331.4	328.6	0.31
20	3	3	315.2	388.5	353.3	365.4	339.1	340.7	338.5	0.30
20	3	4	315.2	388.5	360.0	365.4	349.9	342.2	340.6	0.29
10	0	2	318.4	344.9	340.0	344.9	318.4	320.1	318.6	0.33
10	0	3	323.5	350.7	343.3	350.7	323.5	325.4	323.5	0.33
10	0	4	328.6	356.4	346.7	356.4	328.6	330.5	328.4	0.33

but the former is based on an elastic state of the retained soil.

3.3 Examples from Peng and Chen (2013) under a=0 m and b=∞

In the case of a non-vertical wall back and non-horizontal top surface of the retained cohesionless soil under uniform surcharge (Peng and Chen, 2013), the computation results using the proposed method are given in Table 3. The comparison among various methods indicates that the proposed method agrees well with the other methods.

3.4 Some examples involved in tension cracking

In the case of cohesive soil with relatively small strip surcharge on its top surface, there is tension crack in the soil. Fig. 6 shows a comparison of computed depths of the crack in some examples by the proposed method and some by the classic Rankine-Bell formula (Bell, 1915). It can be seen that the proposed values

Table 2 Active earth thrusts of cohesive soil calculated using different methods (γ=20 kN/m^3, c=10 kPa, φ=30°, δ=10°, ψ=0, H=10 m, α=90°, and β=0°) (Xiao et al., 2021)

q (kPa)	a (m)	b (m)	Active earth thrust (kN/m)					
			Franz G (1983)	45° distribution (Cernica, 1995)	45°+φ/2 distribution (MOHURD, 2013)	Farzaneh et al. (2014)	Proposed	Ratio ξ
10	2	1	241.3	231.2	233.6	210.7	215.6	0.25
20	2	1	254.8	234.5	239.4	216.7	220.7	0.26
30	2	1	268.3	237.9	245.2	222.8	225.6	0.26
20	4	1	270.2	234.5	239.4	216.7	220.7	0.24
50	4	1	333.7	244.5	256.7	235.3	235.5	0.23
100	4	1	439.6	261.2	285.6	267.1	259.1	0.21
20	3	2	274.1	241.2	251.0	228.3	230.6	0.24
20	3	3	285.6	247.9	262.5	235.6	233.1	0.23
20	3	4	297.1	254.5	274.1	235.8	233.1	0.23
10	0	2	233.6	228.8	233.6	216.4	220.7	0.27
10	0	3	239.4	232.1	239.4	221.8	225.7	0.28
10	0	4	245.2	235.4	245.2	227.0	230.5	0.27

Table 3 Active earth pressures of cohesionless soil by various methods (H=10 m, φ=30°, a=0 m, and b=∞) (Peng and Chen, 2013)

γ (kN/m^3)	α (°)	β (°)	δ (°)	q (kPa)	Active earth pressure (kN/m)				
					Coulomb (1776)	Sokolovskii (1965)	Peng and Chen (2013)	Proposed	Ratio ξ
0	90	0	0	20	66.667	66.667	66.667	66.92	0.55
0	78.5	0	20	20	78.107	73.397	78.107	76.59	0.53
0	100	0	10	20	49.015	50.679	51.461	50.39	0.52
20	90	0	0	20	400.000	400.000	400.000	400.06	0.37
20	100	0	0	20	324.338	328.444	328.444	324.01	0.28
20	84.9	0	10	20	413.875	407.587	413.875	411.74	0.41
20	78.5	0	20	20	468.642	440.380	468.643	460.72	0.45
20	90	10	10	20	419.424	413.052	419.424	419.57	0.38
20	90	10	20	0	340.022	320.764	341.349	340.15	0.30
20	83.6	10	20	0	399.559	375.462	399.559	398.32	0.41
20	95.2	10	0	0	334.407	334.407	334.407	334.54	0.35
20	110	10	0	0	234.110	242.602	242.602	234.20	0.17

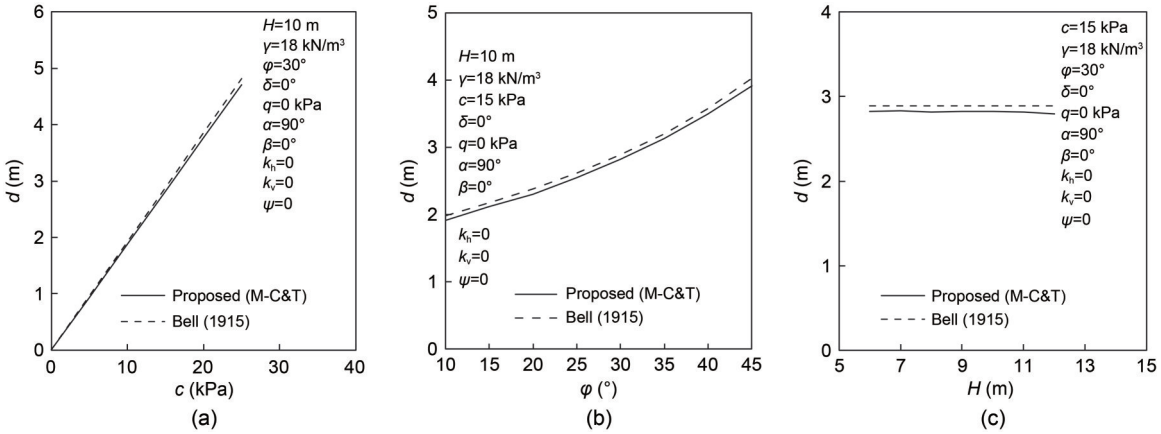

Fig. 6 Comparison of tension crack depths by the proposed method and by the Rankine-Bell formula: (a) *d* vs. *c*; (b) *d* vs. *φ*; (c) *d* vs. *H*

are very slightly smaller than the classical ones in the special cases, which further shows that the proposed method can be generally accepted.

Also, it can be seen from the formula derivation provided above that the proposed method under d=0 m and k_h=k_v=0 can be completely reduced to the simplified method (Xiao et al., 2021), which has already been verified by some tests (Tsagareli, 1965; Tang et al., 1988; Khosravi et al., 2013). This is further evidence for the acceptability of the proposed method.

4 Parametric investigation and discussion

According to the foregoing analysis model and derived formulas, there are generally 13 factors including γ, φ, δ, c, H, β, α, q, a, b, k_h, k_v, and ψ influencing the active earth pressure. So, the influences of these essential factors on the thrust force and failure surface are now individually discussed. For simplicity, the parameters k_h, k_v, ψ, and δ are shown here and the others are shown in the ESM.

4.1 Horizontal seismic coefficient k_h

As shown in Fig. 7, K_a increases non-linearly with k_h, but the minimum value of the ratio ξ is almost linearly increasing as k_h increases. The failure surface in the soil can be approximately regarded as a composite surface with two planes, and it is gradually moving towards the soil interior with the increase of k_h, but the normalized depth of tension crack d/H decreases as k_h increases. Normal stress (compressive stress) on the slip segment OM satisfying the Mohr-Coulomb yield criterion is nearly linearly distributed along the segment under different k_h.

4.2 Vertical seismic coefficient k_v

It can be seen in Fig. 8 that K_a increases linearly with k_v, but the minimum value of the ratio ξ is hardly altered as k_v increases. k_v has almost no influence on the critical sliding surface in the retained soil, but d/H is obviously decreasing as k_v increases. Distribution of normal stress on the shear failure segment of the slip surface still exhibits nearly linear characteristics under different k_v.

4.3 Calibration coefficient of tensile strength cut-off ψ

Fig. 9 shows that ψ has no apparent effect on K_a, but has a noticeable effect on the minimum value of the ratio ξ. As expected, ψ has obvious influence on the location and depth of the tension crack other than the shear segment of the critical slip surface. The location of the tension crack is gradually moving far away from the wall. Besides, normal stress on the shear segment of the slip surface is influenced by ψ to some extent.

4.4 Interface friction angle δ between soil and wall

As can be seen from Fig. 10 that K_a is slightly decreasing with δ/φ, but the minimum value of the ratio ξ is obviously decreasing with δ/φ. The failure surface is developing marginally towards the soil interior as δ/φ increases, and the depth of tension crack is increasing faintly with δ/φ. Distribution of the normal stress σ is nearly linear along the slip segment OM under different values of δ.

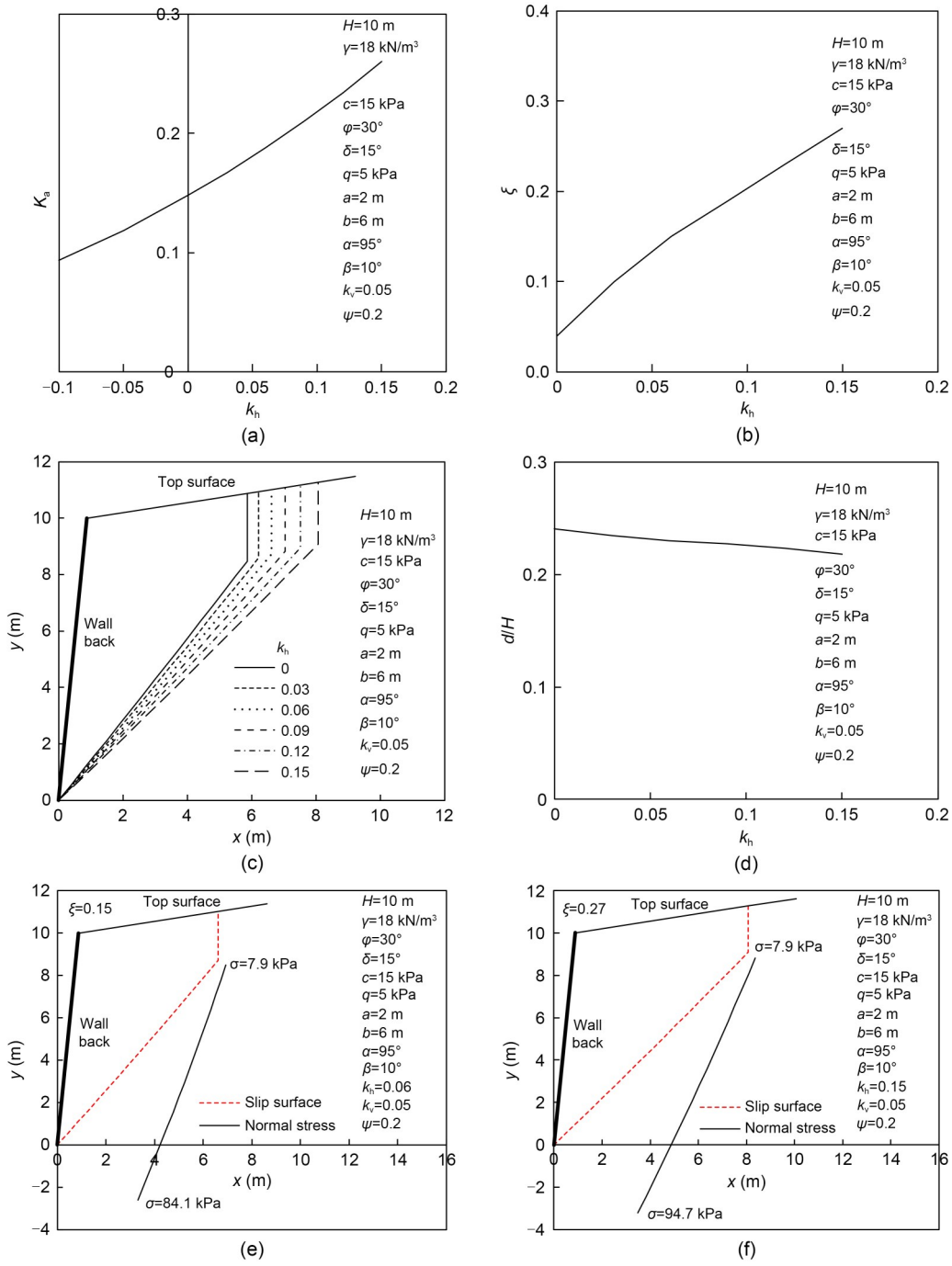

Fig. 7 Influences of k_h on the active earth pressure and other related items: (a) K_a vs. k_h; (b) ξ vs. k_h; (c) slip surfaces; (d) d/H vs. k_h; (e) distribution of normal stress on slip surface under k_h=0.06; (f) distribution of normal stress on slip surface under k_h=0.15

4.5 Ratio of the application point height to wall height ξ

As mentioned above (Fig. 3), the application point of the active thrust from the wall base is rising as the wall purely rotates around the heel, translates, and rotates around the head. Solutions of the ratio ξ controlled by the derived formulas are correspondingly related to various movements of the wall. So, the influence of the ratio ξ on the active earth pressure is further discussed here to reflect the influence of the wall movements. Fig. 11 shows that K_a is nonlinearly

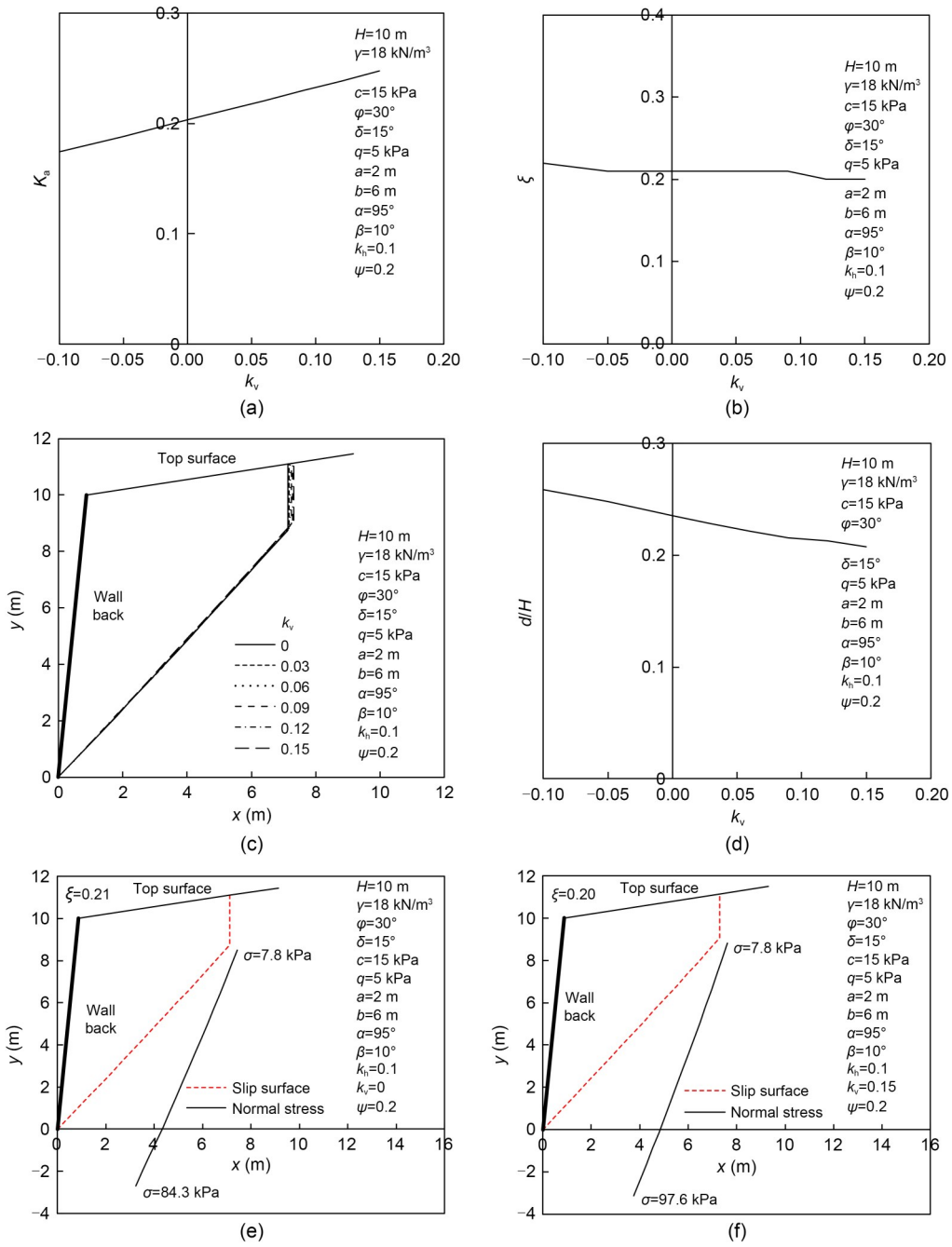

Fig. 8 Influences of k_v on the active earth pressure and other related items: (a) K_a vs. k_v; (b) ξ vs. k_v; (c) slip surfaces; (d) d/H vs. k_v; (e) distribution of normal stress on slip surface under k_v=0; (f) distribution of normal stress on slip surface under k_v=0.15

slightly increasing within a limited range with admissible ratio ξ, which means the active earth pressure is always limited under different possible movements of the same wall. The depth of a tension crack decreases nearly linearly with the increase of the ratio ξ. In particular, the shear slip segment OM of the failure surface varies from planar shape to curved mode as the ratio ξ increases and the slip surface develops gradually towards the wall. Additionally, the ratio ξ has strong influence on the normal stress on the shear slip segment. There are varied characteristics of the slip segment from linear to a curved outline with the increase of the ratio ξ.

Also, according to the proposed method, the application point of Coulomb's active earth pressure can be further discussed. As listed in Table 4 for a typical

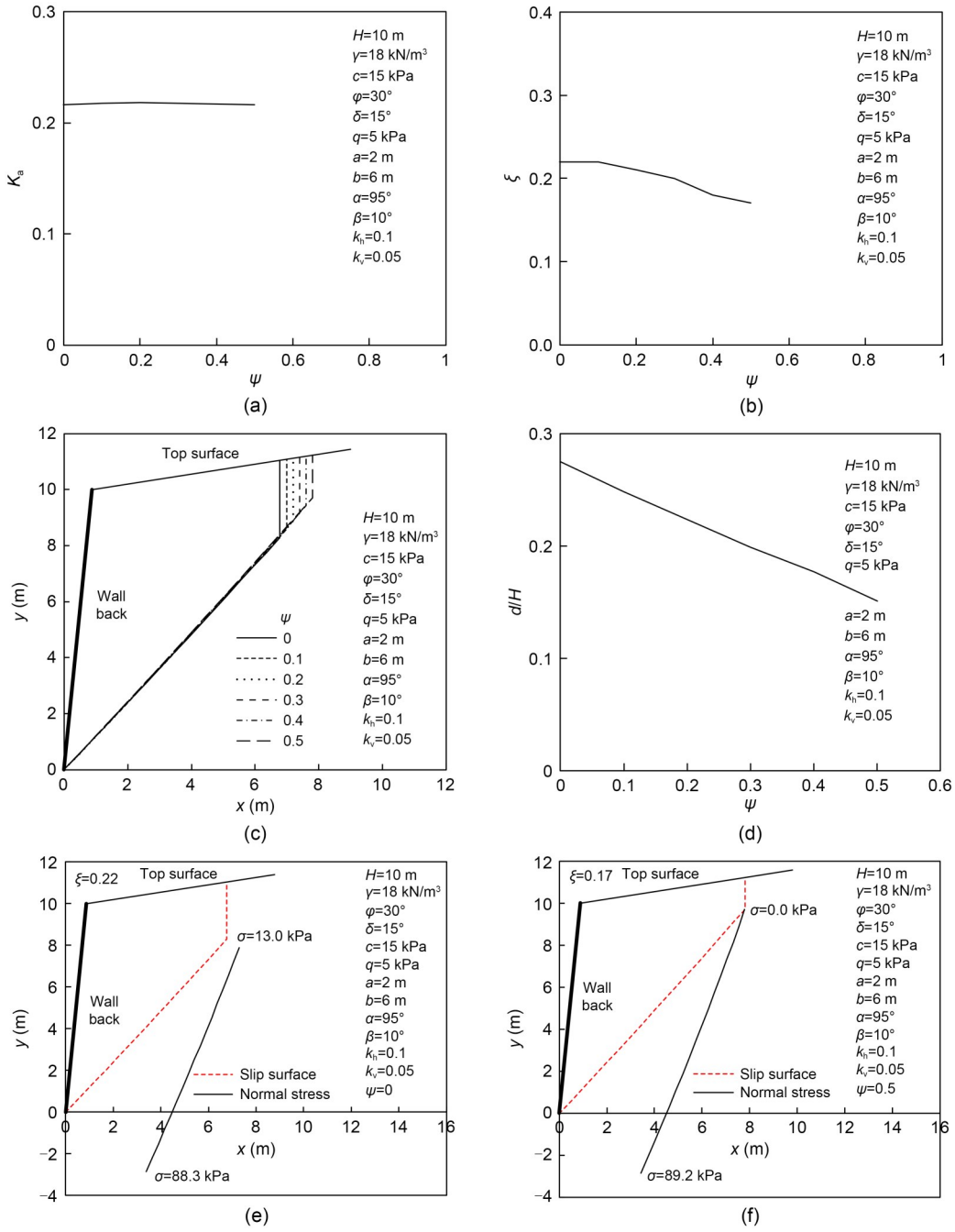

Fig. 9 Influences of ψ on the active earth pressure and other related items: (a) K_a vs. ψ; (b) ξ vs. ψ; (c) slip surfaces; (d) d/H vs. ψ; (e) distribution of normal stress on slip surface under ψ=0; (f) distribution of normal stress on slip surface under ψ=0.5

example with the wall rotation about its base or a point below it, one can see that the application point of the Coulomb's earth pressure is $H/3$ from the wall heel only if δ=0°, α=0°, and β=0°. Actually, whether the application height in the original Coulomb's theory is $H/3$ or not depends on the three angles and the wall movement modes. If δ=0°, α=0°, and β=0°, the active earth pressure increases linearly with depth from zero at the wall top under the wall rotating about its base (Paik and Salgado, 2003). As a result, the application height is exactly $H/3$. However, under the other conditions, the profile of the active earth pressure is not a triangle so that the application height is not equal to $H/3$.

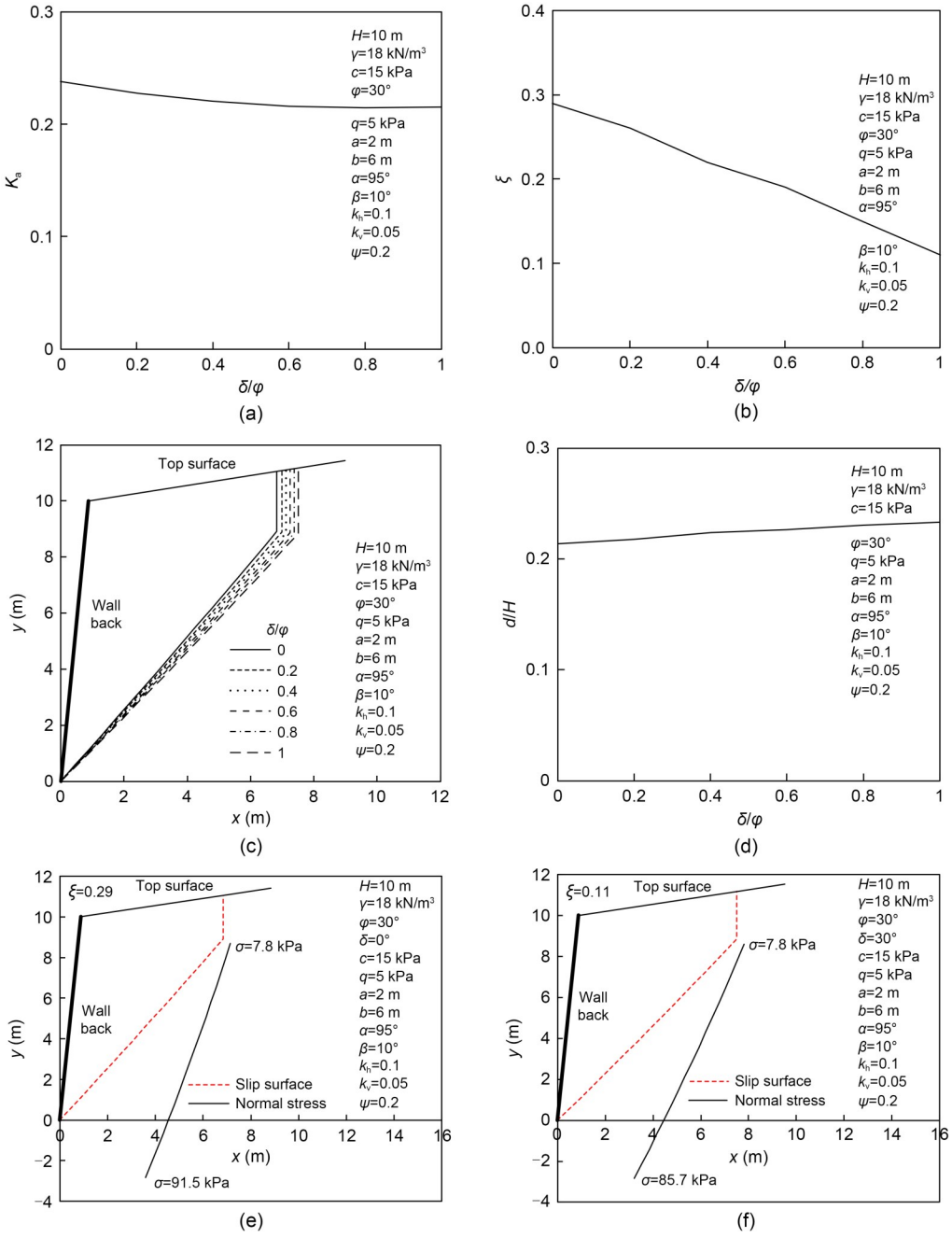

Fig. 10 Influences of δ on the active earth pressure and other related items: (a) K_a vs. δ/φ; (b) ξ vs. δ/φ; (c) slip surfaces; (d) d/H vs. δ/φ; (e) distribution of normal stress on slip surface under δ/φ=0; (f) distribution of normal stress on slip surface under δ/φ=1

5 Conclusions

A general closed-form solution for seismic and static active earth pressure on rigid walls is derived by a variational calculus method broadly considering shear failure together with tension failure of the soil. According to the derived nine dependent equations involved in shear strength and tensile strength cut-off of the soil, the proposed method can be easily executed via an implicit strategy. Compared with some test results and some existing calculation methods, seismic and static active earth pressures computed using the proposed method are in good agreement, which means the proposed method has acceptable accuracy. The

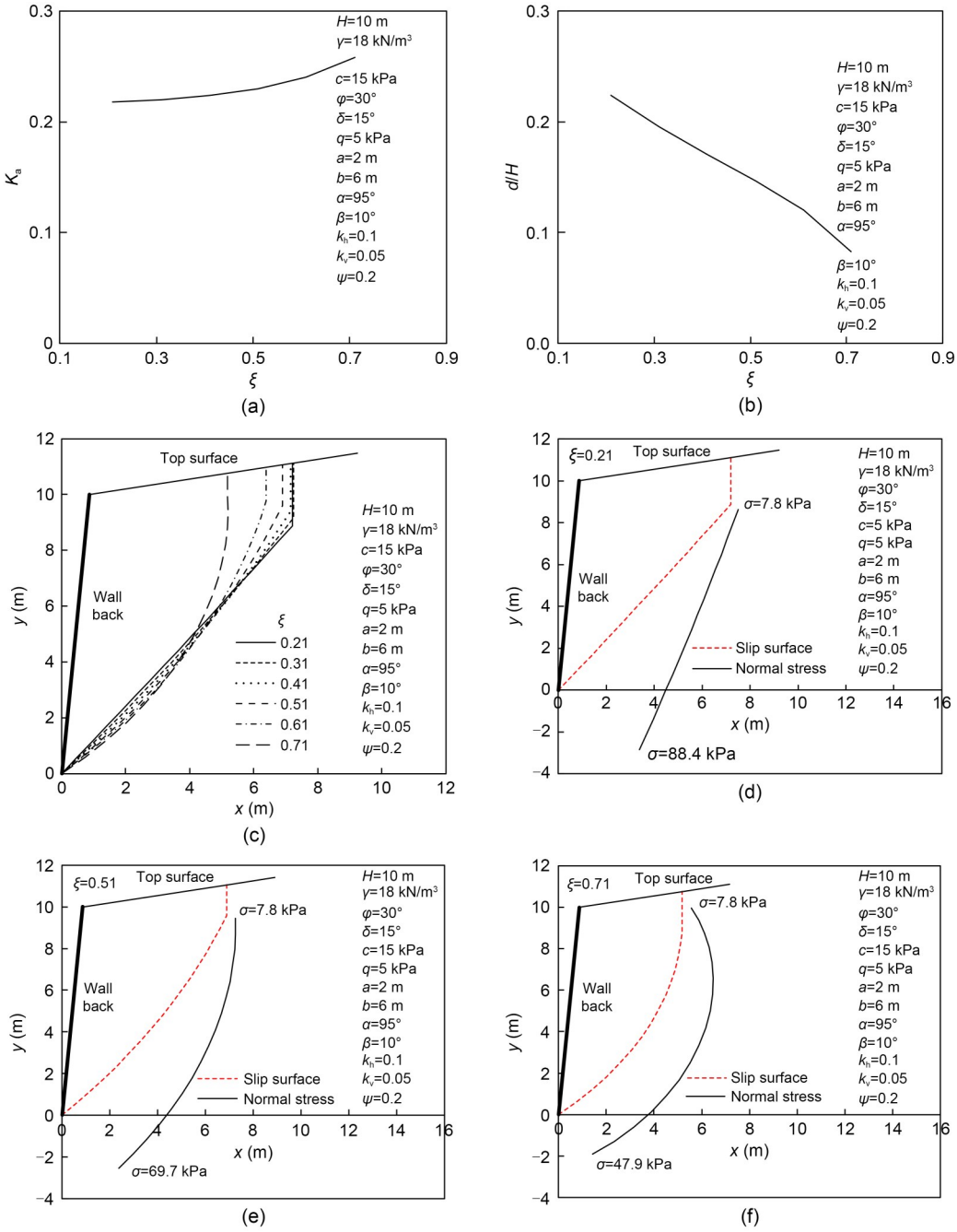

Fig. 11 Influences of the ratio ξ on the active earth pressure and other related items: (a) K_a vs. ξ; (b) d/H vs. ξ; (c) slip surfaces; (d) distribution of normal stress on slip surface under ξ=0.21; (e) distribution of normal stress on slip surface under ξ=0.51; (f) distribution of normal stress on slip surface under ξ=0.71

proposed method can be more extensively used in practice because it does not include assumptions concerning the given shape of the slip surface but gives much more influence to other factors. The proposed method can theoretically determine the variation range of the active earth pressure on a practical rigid wall under possible movements, and quantitatively reveal the influences of 13 basic parameters on the active earth pressure and corresponding failure surface under a specified application point closely related to the possible movement modes of the wall.

Different application points of the earth pressure specified within an admissible range for solving the problem by the proposed method can cause different

Table 4 Application points of active earth pressures under different conditions (γ=18 kN/m^3, φ=30°, c=0, H=10 m, and β=0°)

α (°)	δ (°)	ξ (°)	Proposed E_a (kN/m)	Coulomb's E_a (kN/m)	Relative error (%)
90	0	0.333	300.00	300.00	0.00
90	15	0.309	271.76	271.27	0.18
90	30	0.299	270.83	267.45	1.26
80	0	0.489	356.70	366.03	−2.55
80	30	0.473	376.34	346.26	8.69
100	0	0.325	245.56	243.25	0.95
100	30	0.316	215.20	204.34	5.31

results of the active earth pressure in a limited variety, which physically corresponds to different possible wall movements. The active earth pressure is always in a limited range under different movements of the same wall. Besides, in the case of the lowest value of the application point of the active earth pressure within possible solutions, the critical slip surface in the retained cohesive soil consists usually of a planar shear segment connected with a vertical tension segment near the backfill surface. However, the shear slip segment varies from planar shape to curved mode as the location of the application point rises, and the planar shape of the shear segment is not influenced by the 13 factors.

The tension crack segment of the critical sliding surface in the cohesive soil varies significantly with these factors apart from k_v, a, and b. Similarly, the location of the shear slip segment of the failure surface is not influenced by the five parameters k_v, ψ, q, a, and b.

Seismic active earth pressure increases with k_h and k_v, and the depth of tension crack decreases almost linearly with the two coefficients. The critical sliding surface is progressively moving towards the soil interior with the increase of k_h but is almost uninfluenced by k_v.

Distribution of normal stress on the shear segment of the critical slip surface varies from linear to nonlinear profile along the segment as the ratio ξ increases from its minimum. The magnitude of the normal stress is slightly influenced by ψ, a, and b, but the other parameters also have observable effects on it.

In special cases satisfying Coulomb's assumptions, seismic active earth pressures by the proposed method are very close to those in the improved Mononobe-Okabe method. Moreover, the proposed static active earth pressures under strip surcharge agree well with those by some existing analytical methods related to limit state of the retained soil, but the proposed results are evidently smaller than those by the traditional stress distribution methods based on elasticity theory.

It should be noted that the proposed method can solve the resultant force of the active earth pressure other than the distribution of the earth pressure on the wall, which is its typical limitation and it cannot be used to analyze the internal forces of walls.

Acknowledgments

This work is supported by the National Natural Science Foundation of China (No. 51578466) and the Construction S&T Project of Department of Transportation of Sichuan Province, China (No. 2020A01).

Author contributions

Shiguo XIAO designed the research. Yuan QI and Pan XIA processed the corresponding data. Shiguo XIAO wrote the first draft of the manuscript. Yuan QI and Pan XIA helped to organize the manuscript. Shiguo XIAO revised and edited the final version.

Conflict of interest

Shiguo XIAO, Yuan QI, and Pan XIA declare that they have no conflict of interest.

References

Baker R, Garber M, 1978. Theoretical analysis of the stability of slopes. *Géotechnique*, 28(4):395-411. https://doi.org/10.1680/geot.1978.28.4.395

Bell AL, 1915. The lateral pressure and resistance of clay and the supporting power of clay foundations. *Minutes of the Proceedings of the Institution of Civil Engineers*, 199(1915): 233-272. https://doi.org/10.1680/imotp.1915.16217

Franz G, 1983. Beton Kalender. Verlag von Wilhelm Ernst and Sohn, Munich, Germany (in German).

Cernica JN, 1995. Geotechnical Engineering: Foundation Design. John Wiley & Sons, Inc., New York, USA.

Chang MF, 1997. Lateral earth pressures behind rotating walls. *Canadian Geotechnical Journal*, 34(4):498-509. https://doi.org/10.1139/t97-016

Chen JG, Yang Y, Chen YH, et al., 2020. Calculation of active earth pressure of cohesive soil behind retaining wall considering soil tensile strength. *Rock and Soil Mechanics*, 41(6):1829-1835 (in Chinese). https://doi.org/10.16285/j.rsm.2019.1078

Chen WF, 1975. Limit Analysis and Soil Plasticity. Elsevier, Amsterdam, The Netherlands.

Choudhury D, Singh S, 2006. New approach for estimation of static and seismic active earth pressure. *Geotechnical & Geological Engineering*, 24(1):117-127. https://doi.org/10.1007/s10706-004-2366-x

Coulomb CA, 1776. Essai sur une application des règles de maximis & minimis à quelques problèmes de statique,

relatifs à l'architecture microform. *In*: Mémoires de Mathématique et de Physique. de l'Imprimerie Royale, Paris, France, p.343-382 (in French).

de Josselin de Jong G, 1980. Application of the calculus of variations to the vertical cut off cohesive frictionless soil. *Géotechnique*, 30(1):1-16. https://doi.org/10.1680/geot.1980.30.1.1

Fang YS, Ishibashi I, 1986. Static earth pressures with various wall movements. *Journal of Geotechnical Engineering*, 112(3):317-333. https://doi.org/10.1061/(ASCE)0733-9410(1986)112:3(317)

Fang YS, Chen TJ, 1995. Modification of Mononobe-Okabe theory. *Géotechnique*, 45(1):165-167. https://doi.org/10.1680/geot.1995.45.1.165

Farzaneh O, Askari F, Fatemi J, 2014. Active earth pressure induced by strip loads on a backfill. *International Journal of Civil Engineering*, 12(4):281-291.

Giaquinta M, Hildebrandt S, 2004. Calculus of Variations I. Springer, Berlin, Germany. https://doi.org/10.1007/978-3-662-03278-7

Greco VR, 2006. Lateral earth pressure due to backfill subject to a strip of surcharge. *Geotechnical and Geological Engineering*, 24(3):615-636. https://doi.org/10.1007/s10706-005-2009-x

Han S, Gong JX, Zhang YQ, 2016. Earth pressure of layered soil on retaining structures. *Soil Dynamics and Earthquake Engineering*, 83:33-52. https://doi.org/10.1016/j.soildyn.2015.12.015

Hazarika H, Matsuzawa H, 1996. Wall displacement modes dependent active earth pressure analyses using smeared shear band method with two bands. *Computers and Geotechnics*, 19(3):193-219. https://doi.org/10.1016/0266-352X(96)00003-1

Hou GX, Shu SZ, 2019. Trial wedge approach to determine lateral earth pressures. *International Journal of Geomechanics*, 19(1):06018035. https://doi.org/10.1061/(ASCE)GM.1943-5622.0001326

Iskander M, Chen ZB, Omidvar M, et al., 2013. Active static and seismic earth pressure for *c–φ* soils. *Soils and Foundations*, 53(5):639-652. https://doi.org/10.1016/j.sandf.2013.08.003

Khosravi MH, Pipatpongsa T, Takemura J, 2013. Experimental analysis of earth pressure against rigid retaining walls under translation mode. *Géotechnique*, 63(12):1020-1028. https://doi.org/10.1680/geot.12.P.021

Kim JS, Barker RM, 2002. Effect of live load surcharge on retaining walls and abutments. *Journal of Geotechnical and Geoenvironmental Engineering*, 128(10):803-813. https://doi.org/10.1061/(ASCE)1090-0241(2002)128:10(803)

Kopáscy J, 1957. Three-dimensional stress distribution and slip surfaces in earth works at rupture. Proceedings of the 4th International Conference on Soil Mechanics and Foundations Engineering, p.339-342.

Krabbenhoft K, 2018. Static and seismic earth pressure coefficients for vertical walls with horizontal backfill. *Soil Dynamics and Earthquake Engineering*, 104:403-407. https://doi.org/10.1016/j.soildyn.2017.11.011

Li JP, Wang M, 2014. Simplified method for calculating active earth pressure on rigid retaining walls considering the arching effect under translational mode. *International Journal of Geomechanics*, 14(2):282-290. https://doi.org/10.1061/(ASCE)GM.1943-5622.0000313

Li XG, Liu WN, 2010. Study on the action of the active earth pressure by variational limit equilibrium method. *International Journal for Numerical and Analytical Methods in Geomechanics*, 34(10):991-1008. https://doi.org/10.1002/nag.840

Li XP, Zhao SX, He SM, et al., 2019. Seismic stability analysis of gravity retaining wall supporting *c–φ* soil with cracks. *Soils and Foundations*, 59(4):1103-1111. https://doi.org/10.1016/j.sandf.2019.01.004

Li ZW, Yang XL, 2019. Active earth pressure for retaining structures in cohesive backfills with tensile strength cut-off. *Computers and Geotechnics*, 110:242-250. https://doi.org/10.1016/j.compgeo.2019.02.023

Luan MT, Nogami T, 1997. Variational analysis of earth pressure on a rigid earth-retaining wall. *Journal of Engineering Mechanics*, 123(5):524-530. https://doi.org/10.1061/(ASCE)0733-9399(1997)123:5(524)

Matsuzawa H, Hazarika H, 1996. Analyses of active earth pressure against rigid retaining wall subjected to different modes of movement. *Soils and Foundations*, 36(3):51-65. https://doi.org/10.3208/sandf.36.3_51

Mazindrani ZH, Ganjali MH, 1997. Lateral earth pressure problem of cohesive backfill with inclined surface. *Journal of Geotechnical and Geoenvironmental Engineering*, 123(2):110-112. https://doi.org/10.1061/(ASCE)1090-0241(1997)123:2(110)

Michalowski RL, 2017. Stability of intact slopes with tensile strength cut-off. *Géotechnique*, 67(8):720-727. https://doi.org/10.1680/jgeot.16.P.037

MOHURD (Ministry of Housing and Urban-Rural Development of the People's Republic of China), 2013. Technical Code for Building Slope Engineering, GB 50330-2013. National Standards of the People's Republic of China (in Chinese).

Mononobe N, 1924. Considerations into earthquake vibrations and vibration theories. *Journal of the Japan Society of Civil Engineers*, 10(5):1063-1094.

Nian TK, Han J, 2013. Analytical solution for Rankine's seismic active earth pressure in *c*-ϕ soil with infinite slope. *Journal of Geotechnical and Geoenvironmental Engineering*, 139(9):1611-1616. https://doi.org/10.1061/(ASCE)GT.1943-5606.0000873

Niedostatkiewicz M, Lesniewska D, Tejchman J, 2011. Experimental analysis of shear zone patterns in cohesionless for earth pressure problems using particle image velocimetry. *Strain*, 47(S2):218-231. https://doi.org/10.1111/j.1475-1305.2010.00761.x

Okabe S, Member CE, 1924. General theory on earth pressure and seismic stability of retaining wall and dam. *Journal of the Japan Society of Civil Engineers*, 10(6):1277-1323.

Paik KH, Salgado R, 2003. Estimation of active earth pressure against rigid retaining walls considering arching effects. *Géotechnique*, 53(7):643-653. https://doi.org/10.1680/geot.2003.53.7.643

Park D, Michalowski RL, 2017. Three-dimensional stability analysis of slopes in hard soil/soft rock with tensile strength cut-off. *Engineering Geology*, 229:73-84. https://doi.org/10.1016/j.enggeo.2017.09.018

Paul B, 1961. A modification of the Coulomb-Mohr theory of fracture. *Journal of Applied Mechanics*, 28(2):259-268. https://doi.org/10.1115/1.3641665

Peng MX, Chen J, 2013. Slip-line solution to active earth pressure on retaining walls. *Géotechnique*, 63(12):1008-1019. https://doi.org/10.1680/geot.11.P.135

Puła O, Puła W, Wolny A, 2005. On the variational solution of a limiting equilibrium problem involving an anchored wall. *Computers and Geotechnics*, 32(2):107-121. https://doi.org/10.1016/j.compgeo.2005.01.002

Rankine WJM, 1857. II. On the stability of loose earth. *Philosophical Transactions*, 147:9-27. https://doi.org/10.1098/rstl.1857.0003

Rao PP, Chen QS, Zhou YT, et al., 2016. Determination of active earth pressure on rigid retaining wall considering arching effect in cohesive backfill soil. *International Journal of Geomechanics*, 16(3):04015082. https://doi.org/10.1061/(ASCE)GM.1943-5622.0000589

Richards R, Shi X, 1994. Seismic lateral pressures in soils with cohesion. *Journal of Geotechnical Engineering*, 120(7):1230-1251. https://doi.org/10.1061/(ASCE)0733-9410(1994)120:7(1230)

Saran S, Prakash S, 1968. Dimensionless parameters for static and dynamic earth pressures behind retaining walls. *Indian Geotechnical Journal*, 7(3):295-310.

Shukla SK, Gupta SK, Sivakugan N, 2009. Active earth pressure on retaining wall for c-ϕ soil backfill under seismic loading condition. *Journal of Geotechnical and Geoenvironmental Engineering*, 135(5):690-696. https://doi.org/10.1061/(ASCE)GT.1943-5606.0000003

Sokolovskii VV, 1965. Statics of Granular Media. Pergamon Press, Oxford, UK. https://doi.org/10.1016/C2013-0-02268-2

Soubra AH, Macuh B, 2002. Active and passive earth pressure coefficients by a kinematical approach. *Proceedings of the Institution of Civil Engineers-Geotechnical Engineering*, 155(2):119-131. https://doi.org/10.1680/geng.2002.155.2.119

Spencer E, 1968. Effect of tension on stability of embankments. *Journal of the Soil Mechanics and Foundations Division*, 94(5):1159-1173. https://doi.org/10.1061/JSFEAQ.0001185

Tang ZC, Peng YZ, Song JW, 1988. Centrifuge model test of a rigid wall used to retain cohesionless soil. *Journal of Chongqing Jiaotong University*, 7(2):48-57 (in Chinese).

The MathWorks, Inc., 2018. Global Optimization Toolbox: User's Guide (R2018b). The MathWorks, Inc., Natick, USA. https://www.mathworks.com/help/

Tsagareli ZV, 1965. Experimental investigation of the pressure of a loose medium on retaining walls with a vertical back face and horizontal backfill surface. *Soil Mechanics and Foundation Engineering*, 2(4):197-200. https://doi.org/10.1007/bf01706095

Utili S, 2013. Investigation by limit analysis on the stability of slopes with cracks. *Géotechnique*, 63(2):140-154. https://doi.org/10.1680/geot.11.P.068

Wang YZ, 2000. Distribution of earth pressure on a retaining wall. *Géotechnique*, 50(1):83-88. https://doi.org/10.1680/geot.2000.50.1.83

Wei M, Luo Q, Feng GS, et al., 2022. Shaking table tests on a cantilever retaining wall with reinforced and unreinforced backfill. *Journal of Zhejiang University-SCIENCE A (Applied Physics & Engineering)*, 23(11):900-916. https://doi.org/10.1631/jzus.A2200192

Xiao SG, Yan YP, Xia P, 2021. General solution for active earth pressure on rigid walls under strip surcharge on retained soils using variational method. *International Journal of Civil Engineering*, 19(8):881-896. https://doi.org/10.1007/s40999-020-00579-4

Xie Y, Leshchinsky B, 2016. Active earth pressures from a log-spiral slip surface with arching effects. *Géotechnique Letters*, 6(2):149-155. https://doi.org/10.1680/jgele.16.00015

Yang XL, Zhang S, 2019. Seismic active earth pressure for soils with tension cracks. *International Journal of Geomechanics*, 19(6):06019009. https://doi.org/10.1061/(ASCE)GM.1943-5622.0001414

Zhang F, Leshchinsky D, Baker R, et al., 2016. Implications of variationally derived 3D failure mechanism. *International Journal for Numerical and Analytical Methods in Geomechanics*, 40(18):2514-2531. https://doi.org/10.1002/nag.2543

Zhou YT, Chen QS, Chen FQ, et al., 2018. Active earth pressure on translating rigid retaining structures considering soil arching effect. *European Journal of Environmental and Civil Engineering*, 22(8):910-926. https://doi.org/10.1080/19648189.2016.1229225

Electronic supplementary materials

Sections S1–S7, Eqs. (S1)–(S22)